Wave Motion 46 (2009) 57–73

Contents lists available at ScienceDirect

Wave Motion

journal homepage: www.elsevier.com/locate/wavemoti

The interaction of flexural-gravity waves with periodic geometries

L.G. Bennetts *,[1], N.R.T. Biggs, D. Porter

Department of Mathematics, The University of Reading, PO Box 220, Whiteknights, Reading RG6 6AX, UK

ARTICLE INFO

Article history:
Received 9 January 2008
Received in revised form 29 July 2008
Accepted 7 August 2008
Available online 15 August 2008

Keywords:
Sea-ice
Wave scattering

ABSTRACT

A periodic structure of finite extent is embedded within an otherwise uniform two-dimensional system consisting of finite-depth fluid covered by a thin elastic plate. An incident harmonic flexural-gravity wave is scattered by the structure. By using an approximation to the corresponding linearised boundary value problem that is based on a slowly varying structure in conjunction with a transfer matrix formulation, a method is developed that generates the whole solution from that for just one cycle of the structure, providing both computational savings and insight into the scattering process. Numerical results show that variations in the plate produce strong resonances about the 'Bragg frequencies' for relatively few periods. We find that certain geometrical variations in the plate generate these resonances above the Bragg value, whereas other geometries produce the resonance below the Bragg value. The familiar resonances due to periodic bed undulations tend to be damped by the plate.

1. Introduction

Energy passes through a system comprised of a fluid domain covered by a thin-elastic plate in the form of flexural-gravity waves. These waves manifest themselves as small amplitude oscillations at the interface between the fluid and plate. When a travelling wave meets an inhomogeneity, which in the problem considered herein takes the form of variations in the geometrical surfaces, it is scattered. During the scattering process a number of other motions are generated, and these will be described in detail shortly.

The mathematical model of a thin-elastic plate floating on a fluid domain is used to represent a number of physical situations. Two examples are of particular current interest. The first application is in the area of Very Large Floating Structures (VLFSs), which have, for example, been proposed as offshore runways. The properties of VLFSs are normally uniform. However, as they lie close to land the variations on the ocean floor beneath them are a factor, and ripple beds are a well-known phenomenon. A literature review for VLFSs may be found in [16].

A thin-elastic plate is also used to model sea-ice, which is a relatively thin ice covering and acts as a barrier between the open ocean and the inner land-fast ice. Such coverings may extend over large distances as a quasi-continuous sheet, which contains such inherent non-uniformities as thickness variations. These thickness variations often take the form of a series of undulations, with horizontal length-scales typically of the order kilometres and amplitudes of order metres (see [4]). This adds physical significance to our study of a period structure embedded within a elastic sheet floating on a fluid domain. A summary of the corpus of work existing in this area (until 1995) can be found in [14], and the recent mathematical advances in this general area are reviewed in [13].

* Corresponding author. Tel./fax: +64 34797773.
E-mail addresses: lbennetts@maths.otago.ac.nz (L.G. Bennetts), n.r.t.biggs@rdg.ac.uk (N.R.T. Biggs), d.porter@rdg.ac.uk (D. Porter).
[1] Present address: Department of Mathematics and Statistics, University of Otago, PO Box 56, Dunedin, Otago 9054, New Zealand.

0165-2125/$ - see front matter © 2008 Elsevier B.V. All rights reserved.
doi:10.1016/j.wavemoti.2008.08.002

There already exists a number of notable works on multiple scatterers in this area. For instance, both [15,9] solve for periodic arrays of floes of a finite extent, whilst [6] solves for multiple cracks in an infinite sheet. In [17] multiple thickness variations are considered in a continuous ice covering and a two-dimensional setting, as in this paper, although with the restrictions of zero-draught of the ice sheet and a flat bed. Furthermore, similarly to our work here, an approximation that ignores the effect of evanescent waves between scatterers is considered. It would be possible to adapt our work here to consider a problem in which we have a finite number of identical floes with open water between them and in the far-fields, although we do not pursue this at this stage.

Although we will choose the values of the physical parameters to be those typically used when modelling situations of sea-ice, our focus in this work is on the mathematical aspects of the problem in hand and no further reference to any physical implications will be made. In particular we will be concerned with the generation of Bragg resonance by periodic structures. This phenomenon is well established in situations involving free-surface flows over periodic bedforms (see [8] for example) but has not been studied previously for problems in which the fluid domain is covered by an elastic plate. It is of interest here to investigate both how the presence of an elastic covering affects the response of an incident wave to a periodic bedform and also how an incident wave is scattered by a series of ripples in the plate itself. Moreover, the extension of the unloaded problem to a fluid-plate system is a non-trivial one as we will explain.

Models for free-surface flows over periodic bedforms were derived by both [3,11], amongst others. These two works are cited here as the methods used therein resemble those which will be employed in our work, in that they make use of transition matrices.

A transfer matrix relates the waves to the left of a period to the waves on the right of that period. This is unlike the more familiar scattering matrix, which relates the incoming waves to the outgoing waves. Through use of a transfer matrix, we need only make numerical calculations over one period in order to solve for a structure built up of an arbitrary number of these periods. This therefore creates a large numerical saving when used for periodic structures, as it alleviates the need to discretise the entire interval. Such an approach would be required if we were to solve the problem using the methods of either [12] or [2].

A system comprising an elastic plate floating on fluid differs markedly from the unloaded problem. Unlike a free-surface in which the sole restoring force is provided by gravity, here the flexural response of the sheet is a factor. This leads to a high-order boundary condition, which complicates the solution process.

As in [3] for the periodic bedform with no plate cover, and [12] for non-periodic fluid-plate geometries, we employ a single-mode approximation, in which the vertical mode chosen is that which supports the incident wave. We also note the work of [11], where transfer matrices were used with full-linear theory to solve free-surface problems with periodic bedforms, and [2], who extended the work of [12] to a full linear solution. In doing so the full linear solution may be obtained to any chosen accuracy. However, it has been shown (see [1]) that in the cases considered a single-mode provides high accuracy and its relatively simple structure makes it preferable for our work here.

In addition to the propagating waves, in the case of plate cover the single-mode supports supplementary waves, which have no analogue in the free-surface problem. These waves are generated when a propagating wave meets an obstruction, and will typically be both oscillatory and evanescent. For certain combinations of physical parameters these waves may be purely decaying. Although they are therefore not present at a certain distance away from an obstruction, they will affect the passage of an incident wave and hence the scattering of wave energy.

For the periodic geometry considered in our work here, we will encounter (typically) oscillatory-evanescent waves that are generated as part of the scattering process. Part of our work will be to investigate the effect of the oscillatory-evanescent waves on the scattering process as the propagating waves pass through the periodic structure. To do this we use a simplified model, in which the rôle of the oscillatory-evanescent waves is ignored at the interface between periods.

Our focus for the results presented here is on the phenomenon of Bragg resonance. We show that the resonances generated by ripples in the plate are strong when compared to analogous periodic bedforms in a free-surface context. That is, the resonances have a large capture width even when they are generated by only a relatively small number of ripples. Furthermore, resonance effects are clearly visible in our results up to the tertiary Bragg value.

For water-wave problems with no plate covering it is well known that resonant bands are not typically centred around Bragg values. Instead, they have been observed to appear for slightly longer waves when the periodic structure consists of a series of protrusions on the fluid bed (see [3] for example). Motivated by the finding of this work, the free-surface problem is being revisited by Biggs (in preparation), who will prove in forthcoming work the existence of resonance at slightly shorter wavelengths when the bed contains a series of troughs. These features are reflected in our results where we find that resonances occur for longer waves when the variations involve a thinning of the sheet from the outer states, and similarly for shorter waves when the variations involve a thickening of the sheet. The phenomenon described above increases as the amplitude of the ripples get larger, and we will describe it as *drift*.

The structure of the paper is as follows. In the following section we will outline the mathematical problem to be solved and define the approximation to be used. A solution method based on transfer matrices is then derived in Section 3, and a simplified *plane wave* approximation is formed. Numerical results that concentrate on the production of Bragg resonances are given in Section 4, using our approximations. Finally, in Section 5 our conclusions are made and areas of possible future work are cited.

2. Setting and approximation

We use the Cartesian coordinate x in the horizontal direction and z in the vertical direction, where z points upwards and has its origin set to coincide with the undisturbed fluid surface. A schematic of the hydroelastic system considered is shown in Fig. 1. Although the geometry that is shown in Fig. 1 depicts periodic variations in all of the geometrical surfaces, for the problems considered in the results section of this work, bed and sheet undulations will be dealt with separately. The fluid domain is of infinite extent and is bounded below by an impermeable bed of a finite depth, denoted $z = -h(x)$. An elastic plate of variable thickness $D(x)$ floats on the surface of the fluid. The underside of the plate, $z = -d(x)$, provides an upper boundary to the fluid domain. For convenience, we also define the fluid depth as $H(x) = h(x) - d(x)$. Note that both of the surfaces that bound the fluid above and below are functions of x.

In our model we will permit D, h and d to vary in the finite interval $x \in (0, l)$ only. Outside of this interval all geometrical values are constant and we write $D = D_0$, $H = H_0$, $d = d_0$ and $h = h_0$. The finite interval of varying geometry is constructed of an arbitrary finite number, M, of identical periods. We may therefore subdivide the interval $(0, l)$ accordingly into the M sub-intervals (l_{i-1}, l_i) $(i = 1, \ldots, M)$ where $l_0 = 0$, $l_M = l$, and $l_i - l_{i-1} \equiv l_1 = l/M$ $(i = 1, \ldots, M)$. Moreover, the geometrical variations must satisfy

$$D(x + il_1) = D(x), \quad d(x + il_1) = d(x), \quad h(x + il_1) = h(x) \qquad (i = 1, \ldots, M-1), \text{ for } x \in (0, l_1).$$

We will consider a linear problem, so that perturbations about the equilibrium state are small. It is assumed that the fluid is inviscid, incompressible, homogeneous and in irrotational motion, so that it may be described by a velocity potential $\Phi = \Phi(x, z, t)$, defined so that the velocity is $\nabla\Phi$. When the plate-fluid system is in motion the interface $z = -d$ experiences small amplitude oscillations, and we define the position of the interface at time t as

$$z = -d(x) + \zeta(x, t). \tag{1}$$

If time-harmonic conditions are imposed on the problem then we may write $\Phi(x, z, t) = \Re\mathrm{e}\{(g/\mathrm{i}\omega)\phi(x, z)\mathrm{e}^{\mathrm{i}\omega t}\}$ and $\zeta(x, t) = \Re\mathrm{e}\{\eta(x)\mathrm{e}^{\mathrm{i}\omega t}\}$, for a given angular frequency ω. The unknowns of the problem are now the reduced velocity potential, $\phi(x, z)$, and the reduced displacement of the fluid–ice interface, $\eta(x)$.

Rather than seeking exact solutions for ϕ and η, we will pursue an approximation method. This is based on the restriction of the vertical motion of the fluid structure to the mode that supports propagating waves in the corresponding uniform geometry case and is implemented through a variational principle, which is equivalent to the governing equations of the full linear problem. This defines a mild-slope approximation and was derived in [12]. We therefore introduce the *single-mode approximation* (SMA) of the potential to be

$$\phi(x, z) \approx \varphi(x) w(x, z), \tag{2}$$

where $w(x, z) = \cosh\{k(x)(z + h(x))\}$. Here k is the real root of the dispersion relation

$$(1 - \kappa\alpha + \beta k^4) k \tanh(kH) = \kappa, \tag{3}$$

where $\alpha = \alpha(x) = \rho_p D(x)/\rho_w$ is a scaled version of the mass of the plate, $\beta = \beta(x) = ED^3(x)/12\rho_w g(1 - \nu^2)$ is a scaled version of the flexural rigidity of the plate and $\kappa = \omega^2/g$ is a frequency parameter. The remaining parameters $\rho_p = 922.5$ kg m^{-3} and $\rho_w = 1025$ kgm^{-3} denote the densities of the plate and fluid, respectively, $\nu = 0.3$ is Poisson's ratio, and $E = 5 \times 10^9 Pa$ is Young's modulus for the plate.

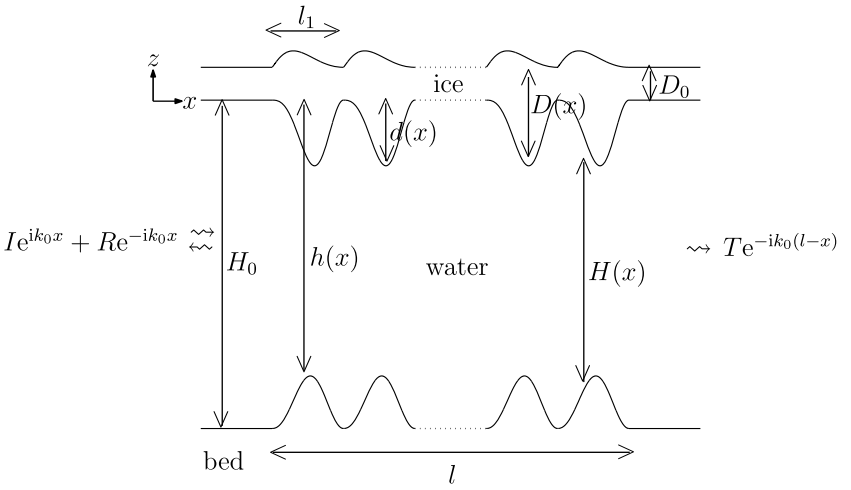

Fig. 1. Schematic of the geometry, showing periodic variations on the upper and lower surfaces of the sheet, and on the bed. In the numerical results generated the sheet and bed variations will be considered separately.

The coupling between ϕ and η implies that when the SMA (2) is made to approximate ϕ the corresponding approximation of the displacement $\eta(x) \approx \chi(x)$ will arise. Unlike the approximation of the velocity potential, the approximation of the displacement occurs indirectly as the displacement function has no vertical dependence.

It is possible to extend the approximation (2) to obtain an arbitrary degree of accuracy by including a finite number of the modes that support evanescent waves. This method has been thoroughly investigated in [1,2]. Although accuracy diminishes for particularly low periods and/or steep geometrical variations, it was shown in these works that our SMA is of high accuracy for parameter values relevant to sea-ice, and in particular for all of the problems that we will consider here.

The governing system of ordinary differential equations for the approximation, which were originally given in [12], are

$$(a(x)\varphi'(x))' + b(x)\varphi(x) + \kappa\cosh(kH)\chi(x) = 0, \tag{4a}$$

and

$$(\beta(x)\chi''(x))'' + (1 - \kappa\alpha(x))\chi(x) - \cosh(kH)\varphi(x) = 0, \tag{4b}$$

where a prime denotes differentiation with respect to x. We choose not to non-dimensionalise in order that the various quantities retain their physical relevance. Suitable non-dimensionalisations for hydroelastic plate equations may be found in [7] or [17].

The values of the coefficients used in Eqs. (4a and 4b) are calculated from

$$a = \frac{1}{4k}(2kH + \sinh(2kH)),$$

and

$$b = k^2 a - (k/2)\sinh(2kH) + (w, w')' - \|w'\|^2.$$

In the above definition of b we have used the inner-product notation

$$(u, v) \equiv \int_{-h(x)}^{-d(x)} u(x, z)v(x, z)\mathrm{d}z,$$

and the corresponding norm notation $\|u\|^2 = (u, u)$, both of which depend on x. An explicit expression for b is given in [12,2].

A single incident wave of unit amplitude propagates from the far left-hand end of the domain ($x \to -\infty$) and is partially reflected and partially transmitted. Therefore, in the far-fields the approximation satisfies the radiation conditions

$$\varphi(x) \sim \begin{cases} Ie^{ik_0x} + Re^{-ik_0x} & (x \to -\infty), \\ Te^{-ik_0(l-x)} & (x \to \infty), \end{cases} \tag{5}$$

where $I = \kappa\mathrm{csch}(k_0H_0)/k_0$ to ensure an incident wave of 1m height, and R and T are, respectively, the reflection and transmission amplitudes that are to be found. The quantity k_0 is the real, positive root k of the dispersion relation (3) in the uniform intervals $x < 0$ and $x > l$.

We note that the radiation conditions (5) have an identical structure to those of the full-linear solution. The only approximation in these limits is in the values of the reflection and transmission coefficients. This is the case because we have used the exact mode that supports the propagating waves in the far-fields, which is actually essential to the formulation of our approximation.

At the edges of the interval of varying geometry, $x = 0, l$, we allow there to be discontinuities in the slope of the surfaces. Eqns. (4a-4b) implicitly assume that the functions d and h are once differentiable and D twice differentiable and do not apply for all points at which these conditions do not hold. We therefore partition $x \in (-\infty, \infty)$ into $x \in (-\infty, 0)$, $x \in (0, l)$ and $x \in (l, \infty)$ to avoid the excluded points.

It is necessary to link the adjacent intervals through jump conditions, which are given in [12] to be

$$\langle\varphi\rangle = 0, \quad \langle\varphi'\rangle = 0 \quad (x = 0, l), \tag{6a}$$

and

$$\langle\chi\rangle = \langle\chi''\rangle = 0, \quad \langle\chi'\rangle = \langle(\beta\chi'')'\rangle = 0 \quad (x = 0, l), \tag{6b}$$

where the notation $\langle\cdot\rangle$ is used to denote the value of the jump in the included quantity. The first of conditions (6a) ensures continuity of fluid pressure at $x = 0, l$, and the second is an approximate form of continuity of fluid flow at $x = 0, l$. Conditions (6b) are similarly the continuity of the position, slope, bending moment and shearing stress of the plate displacement at these points. Even in the case that the geometry is sufficiently differentiable between the varying and uniform states, jump conditions (6a) and (6b) are still applicable and for convenience we will continue to partition the overall interval into the three stated sub-intervals.

At the points between the periods, l_i $(i = 1, \ldots, M - 1)$, we will assume that the geometry is smooth enough that the entire interval of periodic geometry could be solved for without the use of the jump conditions (6a) and (6b). However, as we have already noted, we reject this approach due to our desire to both restrict the number of numerical calculations for periodic geometry and to expose certain features of the scattering process. We note that the continuity of the geometry between

periods is not a necessary condition for the validity of the solution method that we will outline in the following section. More abrupt changes could easily be dealt with, although we would have to use more general jump conditions to (6a) and (6b).

3. Solution using transfer matrices

Our task is now to calculate the quantity φ, which is a component of the approximate potential, along with the approximate displacement function, χ, both of which are functions of x only. To do this we must solve the system of ordinary differential Eqs. (4a) and (4b) in each of the intervals $x \in (-\infty, 0)$, $x \in (0, l)$ and $x \in (l, \infty)$, connect these solutions using the jump conditions (6a) and (6b), and satisfy the radiation conditions (5).

3.1. A general solution procedure

We begin by outlining a solution procedure that is used to calculate the unknown functions.

3.1.1. The intervals of uniform geometry

In intervals of uniform geometry the governing equations simplify due to the constant values taken by the coefficients and it is possible to find an analytical representation for the unknown functions there. The details of the calculation of these forms may be found in [12,2]. Using these forms in the intervals $x \in (-\infty, 0)$ and $x \in (l, \infty)$ and applying the radiation conditions (5) leads to the expressions

$$\varphi(x) = I\mathrm{e}^{\mathrm{i}k_0 x} + R\mathrm{e}^{-\mathrm{i}k_0 x} + \sum_{i=1,2} R_i \mathrm{e}^{-\mathrm{i}\mu_i x} \quad (x < 0), \tag{7a}$$

and

$$\varphi(x) = T\mathrm{e}^{-\mathrm{i}k_0 (l-x)} + \sum_{i=1,2} T_i \mathrm{e}^{-\mathrm{i}\mu_i (l-x)} \quad (x > l), \tag{7b}$$

where R and T are the unknown reflection and transmission amplitudes, respectively. The quantities μ_i $(i = 1, 2)$ are the complex (possibly purely imaginary) roots μ of the quartic equation

$$2a_0(\beta_0\mu^4 + 1 - \alpha_0) + \beta_0 k_0 \sinh(2k_0 H_0)(k_0^2 + \mu^2) = 0,$$

that exist in the upper half complex plane, where, as usual, the subscript 0 indicates that a quantity has been evaluated on a uniform interval. For most combinations of the parameter values the roots μ lie away from the imaginary axis, and these roots are reflections of one another in that axis, i.e. $\mu_2 = -\bar{\mu}_1$. However, when they lie on the imaginary axis the roots μ_i have no clear relation. The conditions under which the position of the roots change are dealt with in [1]. The waves that these roots generate therefore decay exponentially away from the interval of varying geometry but will also oscillate if the real part of μ_i is non-zero. The corresponding amplitudes, R_i and T_i $(i = 1, 2)$, are unknowns. Equivalent expressions for the approximate displacement, χ, can easily be deduced by substituting (7a) and (7b) into (4a) and we find that

$$\chi(x) = \mathrm{e}^{\mathrm{i}k_0 x} + \tilde{R}\mathrm{e}^{-\mathrm{i}k_0 x} + \sum_{i=1,2} \tilde{R}_i \mathrm{e}^{-\mathrm{i}\mu_i x} \quad (x < 0), \tag{8a}$$

and

$$\chi(x) = \tilde{T}\mathrm{e}^{-\mathrm{i}k_0 (l-x)} + \sum_{i=1,2} \tilde{T}_i \mathrm{e}^{-\mathrm{i}\mu_i (l-x)} \quad (x > l), \tag{8b}$$

where $\tilde{R} = R/I$, $\tilde{T} = T/I$, $\tilde{R}_i = (a_0\mu_i^2 - b_0)R_i/\kappa$ and $\tilde{T}_i = (a_0\mu_i^2 - b_0)T_i/\kappa$ $(i = 1, 2)$.

3.1.2. The interval of varying geometry

In the interval of varying geometry, $x \in (0, l)$, where the coefficients are functions of x, it is necessary to calculate the solution numerically. To do this we begin by rewriting the governing Eq. (4) as the second-order matrix system

$$(A(x)\boldsymbol{\Phi}'(x))' + B(x)\boldsymbol{\Phi}(x) = \mathbf{0} \quad (0 < x < l), \tag{9}$$

where $\boldsymbol{\Phi} = (\varphi, \chi, \beta\chi'')^T$, $A = \mathrm{diag}\{a, 1, 1\}$ and

$$B = \begin{pmatrix} b & \kappa\cosh(kH) & 0 \\ 0 & 0 & -\beta^{-1} \\ -\cosh(kH) & 1 - \kappa\alpha & 0 \end{pmatrix}.$$

By applying the second of the jump conditions given in (6a) and (6b) and using the analytic forms (7a), (7b), (8a) and (8b) for $\boldsymbol{\Phi}(0_-)$ and $\boldsymbol{\Phi}(l_+)$, we are able to derive the boundary data

$$\boldsymbol{\Phi}'(0_+) = \mathrm{i}A_0 C_0 K_0 (\mathbf{I} - \mathbf{R}), \quad \boldsymbol{\Phi}'(l_-) = \mathrm{i}A_0 C_0 K_0 \mathbf{T}, \tag{10}$$

where matrix C_0 is defined as $C_0 = [\mathbf{c}(k_0), \mathbf{c}(\mu_1), \mathbf{c}(\mu_2)]$, and for the vectors we have $\mathbf{c}(u) = (1, (a_0u^2 - b_0)/\kappa, -\beta u^2(a_0u^2 - b_0)/\kappa)^T$, $\mathbf{I} = (I, 0, 0)^T$, $\mathbf{R} = (R, R_1, R_2)^T$ and $\mathbf{T} = (T, T_1, T_2)^T$.

The boundary data of Eq. (10) contains six unknown amplitudes through the vectors **R** and **T**. Thus, the vector of solutions, **Φ**, must be determined (up to these unknown constants) as a combination of linearly independent solutions, and we write

$$\mathbf{\Phi}(x) = \mathrm{i}L_-(x)(\mathbf{I} - \mathbf{R}) + \mathrm{i}L_+(x)\mathbf{T} \quad (0 < x < l). \tag{11}$$

In the above expression the quantities $L_\pm$ are 3×3 matrices such that each of their columns satisfies the governing ODE system (9) along with the explicit boundary conditions $L_-(0) = L'_+(l) = A_0C_0K_0$, and $L'_+(0) = L'_-(l) = 0$.

In order to recover the unknown amplitudes, **R** and **T**, we substitute expression (11) into the remaining jump conditions of (6a) and (6b), which, for convenience later, may be written

$$V_0\mathbf{\Phi}(0_+) = V_1(\mathbf{I} + \mathbf{R}), \quad V_0\mathbf{\Phi}(l_-) = V_1\mathbf{T}, \tag{12}$$

where $V_0 = K_0C_0^TA_0\Theta$ and $V_1 = V_0C_0$, with the matrix Θ defined as

$$\Theta = \begin{pmatrix} 1 & 0 & 0 \\ 0 & 0 & -\kappa \\ 0 & -\kappa & 0 \end{pmatrix}. \tag{13}$$

Applying (12) to (11) produces the scattering relation

$$\begin{pmatrix} \mathbf{R} \\ \mathbf{T} \end{pmatrix} = \mathscr{S}\begin{pmatrix} \mathbf{I} \\ \mathbf{0} \end{pmatrix} \tag{14}$$

in which the 6×6 scattering matrix $\mathscr{S}$ is calculated from

$$\mathscr{S} = -(\widetilde{\mathscr{S}}_1 + \mathrm{i}\widetilde{\mathscr{S}}_0)^{-1}(\widetilde{\mathscr{S}}_1 - \mathrm{i}\widetilde{\mathscr{S}}_0), \tag{15}$$

where

$$\widetilde{\mathscr{S}}_0 = \begin{pmatrix} V_0L_-(0) & V_0L_+(0) \\ V_1L_-(l) & V_1L_+(l) \end{pmatrix}, \tag{16}$$

and

$$\widetilde{\mathscr{S}}_1 = \begin{pmatrix} V_1 & 0 \\ 0 & V_1 \end{pmatrix}. \tag{17}$$

The retrieval of **R** and **T** from (14) completes the solution process.

3.2. Formulation of the solution procedure for periodic geometry

The above method of solution is related to those outlined in [12,2]. Although it is possible to obtain a solution using this technique we note that it would involve a discretisation of the entire interval of varying geometry. Our aim is to study the effects of increasing the number of identical periods used and for this reason such a discretisation is impractical here. Instead we will construct a method from which we can easily calculate the SMA for any number of identical periods from the solution of the scattering problem over a single such period alone. This will have the further advantage of allowing for some analytical insight into the phenomenon of resonance, which we anticipate will be a feature of the solution.

3.2.1. Solution over an individual period

From here on, we choose to recast the problem so that the individual period, $x \in (0, l_1)$, is considered fixed and the length of the overall interval of varying geometry $x \in (0, l = Ml_1)$ varies according to the number, M, of periods that constitute it.

So, let us consider the scattering problem posed by an individual period, say the mth period, which occupies the interval (l_{m-1}, l_m), bordered by uniform intervals. We seek the solution to this problem, $\mathbf{\Phi}_m$, over the interval $x \in (l_{m-1} - L, l_m + L)$, where L is some positive finite constant. In the uniform intervals to either side of the period of varying geometry, following (7a) and (7b) and (8a) and (8b) we may write

$$\mathbf{\Phi}_m(x) = \begin{cases} C_0(\mathrm{e}^{\mathrm{i}K_0(x - l_{m-1})}\mathbf{r}_{m-1} + \mathrm{e}^{-\mathrm{i}K_0(x - l_{m-1})}\mathbf{l}_{m-1}) & (l_{m-1} - L < x < l_{m-1}), \\ C_0(\mathrm{e}^{\mathrm{i}K_0(l_m x)}\mathbf{l}_m + \mathrm{e}^{-\mathrm{i}K_0(l_m - x)}\mathbf{r}_m) & (l_m < x < l_m + L), \end{cases} \tag{18}$$

where $\mathrm{e}^{\mathrm{i}K_0x} = \mathrm{diag}\{\mathrm{e}^{\mathrm{i}k_0x}, \mathrm{e}^{\mathrm{i}\mu_1x}, \mathrm{e}^{\mathrm{i}\mu_2x}\}$ and the $\mathbf{l}_i$ and $\mathbf{r}_i$ $(i = m - 1, m)$ are constant vectors that contain the amplitudes of the leftward and rightward travelling waves, respectively.

The solution $\mathbf{\Phi}_m$ is then obtained using the method that was described earlier, in Section 3.1, where we must simply transfer the period of geometry in (l_{m-1}, l_m) here onto the interval $(0, l_1)$ and calculate the matrices of linearly independent solutions $L_{\pm,m} \equiv L_\pm$ to this problem. Here we set the constant $L = 0$, so that the periods occur contiguously. Doing so, we define the scattering relation

$$\begin{pmatrix} \mathbf{l}_{m-1} \\ \mathbf{r}_m \end{pmatrix} = \mathscr{S}_m \begin{pmatrix} \mathbf{r}_{m-1} \\ \mathbf{l}_m \end{pmatrix}, \tag{19}$$

where the scattering matrix $\mathscr{S}_m$ is found from (15) to (17), the only proviso being that the linearly independent solutions $L_{\pm,m}$ replace $L_\pm$ in (16).

3.2.2. Solution for an arbitrary number of periods

In (19) the unknown amplitudes are related through a scattering matrix, so that the outgoing amplitudes are given in terms of the incoming amplitudes. Equivalently we may relate them through a transfer matrix, $\mathscr{P}_m$, where the amplitudes to the right of the period are given in terms of the amplitudes to the left of the period, so that

$$\begin{pmatrix} \mathbf{r}_m \\ \mathbf{l}_m \end{pmatrix} = \mathscr{P}_m \begin{pmatrix} \mathbf{r}_{m-1} \\ \mathbf{l}_{m-1} \end{pmatrix}. \tag{20}$$

The transfer matrix $\mathscr{P}_m$ may be calculated from

$$\mathscr{P}_m = -\widetilde{\mathscr{P}}_{m,0}^{-1}\widetilde{\mathscr{P}}_{m,1},$$

where

$$\widetilde{\mathscr{P}}_{m,0} = \begin{pmatrix} \mathrm{i}V_1 L_{-,m}(l_{m-1}) & -\mathrm{i}V_1 L_{-,m}(l_{m-1}) \\ V_0 + \mathrm{i}V_1 L_{-,m}(l_m) & V_0 - \mathrm{i}V_1 L_{-,m}(l_m) \end{pmatrix},$$

and

$$\widetilde{\mathscr{P}}_{m,1} = \begin{pmatrix} V_0 - \mathrm{i}V_1 L_{+,m}(l_{m-1}) & V_0 + \mathrm{i}V_1 L_{+,m}(l_{m-1}) \\ \mathrm{i}V_1 L_{+,m}(l_m) & -\mathrm{i}V_1 L_{+,m}(l_m) \end{pmatrix}.$$

Alternatively we may deduce the transfer matrix from the scattering matrix and vice versa by using the expressions

$$\mathscr{S}_m = \begin{pmatrix} \mathscr{R}_{m,-} & \mathscr{T}_{m,+} \\ \mathscr{T}_{m,-} & \mathscr{R}_{m,+} \end{pmatrix}, \tag{21}$$

and

$$\mathscr{P}_m = \begin{pmatrix} \mathscr{T}_{m,-} - \mathscr{R}_{m,+}\mathscr{T}_{m,+}^{-1}\mathscr{R}_{m,-} & \mathscr{R}_{m,+}\mathscr{T}_{m,+}^{-1} \\ -\mathscr{T}_{m,+}^{-1}\mathscr{R}_{m,-} & \mathscr{T}_{m,+}^{-1} \end{pmatrix}, \tag{22}$$

where the $\mathscr{R}_{m,\pm}$ and $\mathscr{T}_{m,\pm}$ are 3×3 matrices of reflection and transmission coefficients, which may be calculated from Eqs. (15)–(17).

Now, let us return to the situation of an interval of geometry that comprises M identical periods adjacent to one another. The scattering problem posed by the entire interval consists of the individual response of each period along with the interaction of the periods. Therefore, the mth period may be considered to be forced by the outgoing waves from its adjacent periods, namely $\mathbf{r}_{m-1}$ and $\mathbf{l}_m$, with its outgoing waves, $\mathbf{l}_{m-1}$ and $\mathbf{r}_m$, concomitantly providing partial forcing for these adjacent periods.

Using the definition of the transfer matrix (20), we therefore have

$$\begin{aligned} \begin{pmatrix} \mathbf{T} \\ \mathbf{0} \end{pmatrix} = \begin{pmatrix} \mathbf{r}_M \\ \mathbf{l}_M \end{pmatrix} &= \mathscr{P}_M \begin{pmatrix} \mathbf{r}_{M-1} \\ \mathbf{l}_{M-1} \end{pmatrix} \\ &= \mathscr{P}_M\mathscr{P}_{M-1} \begin{pmatrix} \mathbf{r}_{M-2} \\ \mathbf{l}_{M-2} \end{pmatrix} \\ &\vdots \\ &= \mathscr{P}_M\mathscr{P}_{M-1}\ldots\mathscr{P}_1 \begin{pmatrix} \mathbf{r}_0 \\ \mathbf{l}_0 \end{pmatrix} = \mathscr{P}_M\mathscr{P}_{M-1}\ldots\mathscr{P}_1 \begin{pmatrix} \mathbf{I} \\ \mathbf{R} \end{pmatrix}, \end{aligned} \tag{23}$$

where we have matched the outermost rightward and leftward amplitudes to the reflected and transmitted amplitudes of the entire interval as defined in Eqs. (7a) and (7b) and (8a) and (8b). Furthermore, as each period is identical the transfer matrices are the same, so that $\mathscr{P}_1 = \mathscr{P}_2 = \ldots = \mathscr{P}_M$. Here, we highlight the fact that the phase changes that occur between periods have been accounted for in the definition of the amplitudes in Eq. (18). Thus the transfer matrix for the entire interval, which we denote $\mathscr{P}$, is given by the simple expression

$$\mathscr{P} = \mathscr{P}_1^M. \tag{24}$$

It is then possible to recover the scattering matrix for the entire interval, $\mathscr{S}$, from the transfer matrix $\mathscr{P}$ given in (24) by using the relations that are analogous to those of the single period, given in Eqs. (21) and (22).

Of course, in the formulation of (23) there is no requirement that the geometry be periodic, and it gives a means for solving for more general multiple scatterers. This is not the focus of our present work, which is concerned with the features that result from considering periodic geometries. However, the more general non-periodic case will be investigated in work that is currently in preparation.

In Eq. (24) we have a means of calculating the scattering properties of an interval of varying geometry, which is composed of an arbitrary number of identical periods from only one solution of the scattering problem defined by a single such period. Note also that in order to derive the result (24), we have assumed that the geometry is smooth at the interfaces between adjacent periods. However, expression (24) is unchanged if we were to suppose that the geometry is not differentiable at these points, as we noted earlier.

3.3. The transfer matrix

As the use of a transfer matrix forms the basis for our solution method, we discuss here a few of its properties. So, consider again the scattering problem posed by the mth period of varying geometry and its solution $\mathbf{\Phi}_m$ and associated transfer matrix $\mathscr{P}_m$.

To deduce the first property, we note that the coefficients of the governing system of Eqs. (9) and (10) are real-valued. We may then take complex conjugates and find that $\overline{\mathbf{\Phi}}_m$ satisfies the same scattering problem, although we must make the appropriate changes to the amplitudes of the incoming and outgoing waves. That is, the propagating waves switch directions so that outgoing becomes incoming and vice versa. If the roots μ_i $(i = 1, 2)$ lie away from the imaginary axis then they create oscillatory-evanescent waves, which also switch direction, but if they are purely imaginary then they generate evanescent waves that do not vary under conjugation. Therefore, the transfer relation for the conjugate problem is

$$\mathscr{I}\begin{pmatrix}\overline{\mathbf{r}}_m\\ \overline{\mathbf{I}}_m\end{pmatrix} = \mathscr{P}_m\mathscr{I}\begin{pmatrix}\overline{\mathbf{r}}_{m-1}\\ \overline{\mathbf{I}}_{m-1}\end{pmatrix}, \tag{25}$$

for the transfer matrix $\mathscr{P}_m$ defined in Eq. (20). The matrix $\mathscr{I}$ is defined as either

$$\mathscr{I} = \begin{pmatrix}0&0&0&1&0&0\\0&0&0&0&0&1\\0&0&0&0&1&0\\1&0&0&0&0&0\\0&0&1&0&0&0\\0&1&0&0&0&0\end{pmatrix} \quad \text{or} \quad \mathscr{I} = \begin{pmatrix}0&0&0&1&0&0\\0&1&0&0&0&0\\0&0&1&0&0&0\\1&0&0&0&0&0\\0&0&0&0&1&0\\0&0&0&0&0&1\end{pmatrix}$$

depending on whether the roots μ_i $(i = 1, 2)$ lie off or on the imaginary axis, respectively. In either case $\mathscr{I}$ is self-inverse and by comparing (20) and (25) we derive the relationship

$$\mathscr{P}_m = \mathscr{I}\overline{\mathscr{P}}_m\mathscr{I},$$

which implies that the eigenvalues of the transfer matrix $\mathscr{P}_m$ are real-valued or arise in complex conjugate pairs. The identical property was proved by Porter and Porter [11] for free-surface flows over periodically undulating beds.

A second property results from the identities

$$V_1L_{+,m}(l_{m-1}) = (V_1L_{+,m}(l_{m-1}))^T, \quad V_1L_{-,m}(l_m) = (V_1L_{-,m}(l_m))^T, \tag{26a}$$

and

$$V_1L_{+,m}(l_m) = (V_1L_{-,m}(l_{m-1}))^T. \tag{26b}$$

These are proved in Appendix B of [1] and make use of the energy balance

$$\left[\mathbf{\Phi}_{(1)}^T\Theta A\mathbf{\Phi}'_{(0)} - \mathbf{\Phi}_{(1)}'^T\Theta A\mathbf{\Phi}_{(0)}\right]_{x_0}^{x_1} = 0,$$

where Θ is defined in Eq. (13). This energy balance was first given in [12] for solutions $\mathbf{\Phi}_{(i)}(i = 0, 1)$ of (9) and arbitrary points $x_i(i = 0, 1)$. Identities (26a-26b) may be used directly to establish the equality

$$\widetilde{\mathscr{P}}_{m,1}\widetilde{S}_2^{-1}\widetilde{\mathscr{P}}_{m,1}^T = \widetilde{\mathscr{P}}_{m,0}\widetilde{\mathscr{S}}_2^{-1}\widetilde{\mathscr{P}}_{m,0}^T$$

where

$$\widetilde{\mathscr{S}}_2 = \begin{pmatrix}0&V_1\\-V_1&0\end{pmatrix},$$

and consequently we find that

$$\mathscr{P}_m^T = \widetilde{\mathscr{S}}_2\mathscr{P}_m^{-1}\widetilde{\mathscr{S}}_2^{-1}. \tag{27}$$

From Eq. (27) we may conclude that the eigenvalues of the transfer matrix $\mathscr{P}_m$ arise in reciprocal pairs. Again, this property has been proved in [11] for free-surface flows.

We can use the equality (27) to calculate an auxiliary result. Consider the transfer matrix that gives the left-hand amplitudes in terms of the right-hand amplitudes, rather than $\mathscr{P}_m$ that works the opposite way around. Calculation of this matrix can be achieved in two ways: firstly, in analogous fashion to the derivation of $\mathscr{P}_m$ in (22), we may write

$$\begin{pmatrix} \mathbf{l}_{m-1} \\ \mathbf{r}_{m-1} \end{pmatrix} = \begin{pmatrix} \mathscr{T}_{m,+} - \mathscr{R}_{m,-}\mathscr{T}_{m,-}^{-1}\mathscr{R}_{m,+} & \mathscr{R}_{m,-}\mathscr{T}_{m,-}^{-1} \\ -\mathscr{T}_{m,-}^{-1}\mathscr{R}_{m,+} & \mathscr{T}_{m,-}^{-1} \end{pmatrix} \begin{pmatrix} \mathbf{l}_m \\ \mathbf{r}_m \end{pmatrix}. \tag{28a}$$

Alternatively, we may calculate the right-to-left transfer matrix in terms of the inverse of $\mathscr{P}_m$, with

$$\begin{pmatrix} \mathbf{l}_{m-1} \\ \mathbf{r}_{m-1} \end{pmatrix} = \begin{pmatrix} 0 & I_3 \\ I_3 & 0 \end{pmatrix} \mathscr{P}_m^{-1} \begin{pmatrix} 0 & I_3 \\ I_3 & 0 \end{pmatrix} \begin{pmatrix} \mathbf{l}_m \\ \mathbf{r}_m \end{pmatrix}, \tag{28b}$$

where I_3 is the 3×3 identity matrix. Comparing (28a) and (28b) and using Eq. (27) we have the equality

$$\begin{pmatrix} \mathscr{T}_{m,+} - \mathscr{R}_{m,-}\mathscr{T}_{m,-}^{-1}\mathscr{R}_{m,+} & \mathscr{R}_{m,-}\mathscr{T}_{m,-}^{-1} \\ -\mathscr{T}_{m,-}^{-1}\mathscr{R}_{m,+} & \mathscr{T}_{m,-}^{-1} \end{pmatrix} = \begin{pmatrix} I_3 & 0 \\ 0 & I_3 \end{pmatrix} \widetilde{\mathscr{S}}_2^{-1} \mathscr{P}_m^T \widetilde{\mathscr{S}}_2 \begin{pmatrix} I_3 & 0 \\ 0 & I_3 \end{pmatrix}. \tag{29}$$

Now matching block entries in Eq. (29) gives a set of four identities, and we note in particular that $\mathscr{T}_{m,+}V_1 = V_1\mathscr{T}_{m,-}$, which implies that $\mathrm{diag}(\mathscr{T}_{m,-}) = \mathrm{diag}(\mathscr{T}_{m,+})$.

The conjugate and reciprocal properties of the eigenvalues of the transfer matrix are of practical importance for our solution procedure. Following [11] we use these properties to decompose the transfer matrix as

$$\mathscr{P}_1 = \mathscr{P}_2 = \ldots \mathscr{P}_M = \mathscr{H} \begin{pmatrix} \Delta & 0 \\ 0 & \Delta^{-1} \end{pmatrix} \mathscr{H}^{-1} \tag{30}$$

where Δ is a diagonal matrix containing the eigenvalues of $\mathscr{P}_1 = \mathscr{P}_2 = \ldots \mathscr{P}_M$ that are of magnitude less than unity or that lie on the upper half of the unit circle. The matrix $\mathscr{H}$ contains the eigenvectors of the transfer matrix.

Referring to Eq. (24), the transfer matrix for the interval composed of M periods is given from expression (30) as

$$\mathscr{P} = \mathscr{P}_1^M = \mathscr{H} \begin{pmatrix} \Delta^M & 0 \\ 0 & \Delta^{-M} \end{pmatrix} \mathscr{H}^{-1}, \tag{31}$$

from which the scattering matrix for the entire interval, $\mathscr{S}$, may be obtained through Eqs. (21) and (22). However, as the terms in Δ^M are decaying and the terms in Δ^{-M} growing, we anticipate the likelihood of extreme values for large M. In order to avoid the numerical difficulties that this would cause, we mimic [11] by calculating the scattering matrix from

$$\mathscr{S} = -\begin{pmatrix} \mathscr{H}_{22} & -\Delta^M\mathscr{H}_{21} \\ \Delta^M\mathscr{H}_{12} & -\mathscr{H}_{11} \end{pmatrix}^{-1} \begin{pmatrix} \mathscr{H}_{21} & -\Delta^M\mathscr{H}_{22} \\ \Delta^M\mathscr{H}_{11} & -\mathscr{H}_{12} \end{pmatrix}, \tag{32}$$

where the 3×3 matrices $\mathscr{H}_{ij}$ are defined through

$$\mathscr{H}^{-1} = \begin{pmatrix} \mathscr{H}_{11} & \mathscr{H}_{12} \\ \mathscr{H}_{21} & \mathscr{H}_{22} \end{pmatrix}.$$

Similarly, the amplitudes are retrieved by simultaneously solving the relations

$$\left.\begin{aligned} \mathscr{H}_{11}\mathbf{r}_i + \mathscr{H}_{12}\mathbf{l}_i &= \Delta\mathscr{H}_{11}\mathbf{r}_{i-1} + \Delta\mathscr{H}_{12}\mathbf{l}_{i-1} \\ \Delta\mathscr{H}_{21}\mathbf{r}_i + \Delta\mathscr{H}_{22}\mathbf{l}_i &= \mathscr{H}_{21}\mathbf{r}_{i-1} + \mathscr{H}_{22}\mathbf{l}_{i-1} \end{aligned}\right\} \quad (i = 1, \ldots, M). \tag{33}$$

In Eqs. (31)–(33) we have a means of calculating the solution for the entire interval of varying geometry, comprised of an arbitrary number of identical periods, from knowledge of the transfer matrix for a single period. In particular, we have derived an efficient method of extending the transfer matrix for a single period to multiple periods through its eigenvalues and eigenvectors. These quantities depend on the geometry of the individual period and on the frequency of the problem. For a fixed geometry then, the eigenvalues (and eigenvectors) may be regarded as functions of frequency.

From previous study of free-surface problems over undulating topography, we may expect to find that, as the frequency parameter varies, two of these eigenvalues will typically almost entirely circumnavigate the perimeter of the unit circle as a conjugate pair. Furthermore, we expect that, as the paths of these eigenvalues meet on the real axis, the eigenvalues will depart from the unit circle for a finite frequency interval, forming a real reciprocal pair. In such a situation there will be growing terms in Δ^{-M} as the number of periods, M, increases. From expression (32) we can infer that this is likely to amplify terms in the scattering matrix and lead to resonance.

3.4. Simplification via restriction to the plane wave only

The calculation of the scattering matrix $\mathscr{S}$ from Eq. (32) requires the inversion of a 6×6 matrix. This makes the explicit calculation of the scattering coefficients somewhat abstruse and the analysis of the phenomenon of resonance difficult. Therefore, it is difficult to substantiate the suppositions we made regarding the eigenvalues and resonance at the end of the last section.

Instead, we shall simplify matters by making the assumption that the interactions between adjacent periods involve only the propagating waves and neglect the rôle of the oscillatory-evanescent/evanescent waves, which have wavenumbers μ_i $(i = 1, 2)$ at these points. This reduces the dimension of the scattering problem that we must determine from six to two, allowing for some analytical insight to be gained.

As mentioned earlier, the evanescent waves which are supported by the propagating wave-bearing eigenfunction, are generated by the high-order boundary condition. These waves have no analogue in the free-surface problem in which the SMA produces only propagating waves. However, ignoring them in the elastic-plate problem is an additional approximation to that of the SMA.

Such an approximation is often termed as a *wide spacing approximation*. However, this description is misleading in this instance as the periods are not separated. Instead we adopt the description *plane wave approximation* (PWA). In the following section we will compare the results produced by the full approximation (SMA) and the simplified approximation (PWA) and will find that the performance of the latter is good, which supports its use.

Approximations analogous to the PWA have been used previously for free-surface flows with periodic bedforms (see [3]). We may therefore refer to the work of these authors and merely quote the pertinent results here.

By restricting the 6×6 scattering matrix for an individual period, $\mathscr{S}_m$, to the 2×2 scattering matrix for the period

$$S_m = \begin{pmatrix} R_{m,-} & T_m \\ T_m & R_{m,+} \end{pmatrix},$$

we calculate an approximate version of the transfer matrix for the period restricted to the propagating waves

$$P_m = T_m^{-1} \begin{pmatrix} -\det(S_m) & R_{m,+} \\ -R_{m,-} & 1 \end{pmatrix}.$$

Using an identical method of finding the scattering characteristics for the entire interval as outlined in Eqs. (31)–(32), we deduce the following plane wave approximation for the scattering matrix over the entire interval of periods, S, to be

$$S \approx -\begin{pmatrix} -R_{1,+} & \mathrm{e}^{\mathrm{i}M\lambda}(1 - T_1\mathrm{e}^{-\mathrm{i}\lambda}) \\ \mathrm{e}^{\mathrm{i}M\lambda}(1 - T_1\mathrm{e}^{\mathrm{i}\lambda}) & -R_{1,+} \end{pmatrix}^{-1} \begin{pmatrix} (1 - T_1\mathrm{e}^{-\mathrm{i}\lambda}) & -\mathrm{e}^{\mathrm{i}M\lambda}R_{1,+} \\ -\mathrm{e}^{\mathrm{i}M\lambda}R_{1,+} & (1 - T_1\mathrm{e}^{\mathrm{i}\lambda}) \end{pmatrix}. \tag{34}$$

Here, $\mathrm{e}^{\pm\mathrm{i}\lambda}$ represent the eigenvalues of the transfer matrix P_m, where λ is calculated from

$$\cos(\lambda) = \frac{\cos(\arg T_m)}{|T_m|}. \tag{35}$$

In expression (34) we have approximations for the modulus of the transmission coefficient T/I (see (5)),

$$|T/I|^2 \approx |\widehat{T}|^2 = \frac{|T_1|^2 \sin^2(\lambda)}{|T_1|^2 \sin^2(\lambda) + |R_{1,\pm}|^2 \sin^2(M\lambda)}. \tag{36}$$

Using the energy equation $|R/I|^2 = 1 - |T|^2$ then gives an approximation for the modulus of the reflection coefficient

$$|R/I|^2 \approx |\widehat{R}|^2 = \frac{|R_{1,\pm}|^2 \sin^2(M\lambda)}{|T_1|^2 \sin^2(\lambda) + |R_{1,\pm}|^2 \sin^2(M\lambda)}.$$

There are now two different possibilities depending on the form of the eigenvalue parameter λ. If λ is real then the above expressions (36) will oscillate boundedly, and [11] gave the bounding envelopes

$$|\widehat{T}|^2 \geqslant \frac{|T|^2 \sin^2(\lambda)}{|T|^2 \sin^2(\lambda) + |R|^2} \quad (M = 1, 2, \ldots),$$

and

$$|\widehat{R}|^2 \leqslant \frac{|R|^2}{|T|^2 \sin^2(\lambda) + |R|^2} \quad (M = 1, 2, \ldots), \tag{37}$$

for this situation. However, if λ possesses an imaginary part then $\sin(M\lambda)$ is unbounded as M increases and consequently $|\widehat{T}| \to 0$ and $|\widehat{R}| \to 1$ as $M \to \infty$. Thus, in cases of λ not being real-valued, we attain resonance as the number of periods increases and the rate at which it is attained is dependent on the value of $|R_{1,\pm}|$ and the size of the imaginary part of λ.

We note that there is a further numerical saving possible in using the PWA. This is in the calculation of the SMA, $\mathbf{\Phi}_1$, over a single period of varying geometry from which we form the required transfer matrix P_1. As we are only considering the interaction of propagating waves between periods, it is only necessary to solve for two linearly independent solutions to form $\mathbf{\Phi}_1$. This method is outlined in Section 6.1 of [2].

4. Numerical results

In this section we are particularly concerned with the phenomenon of resonance, which is well known to occur in other water-wave problems involving periodic structures around the so-called Bragg values $K \equiv k_0 l_1/\pi = 1, 2, \ldots$. The results that we give here will demonstrate the existence of exactly these Bragg resonance in the current setting of a floating elastic plate where the physical parameters used are those given in Section 2. Features of *leftward drift* and *rightward drift* of the resonance bands, as the amplitude of the obstruction increases, will also arise.

Before conducting our investigations into resonance we make a brief diversion in order to validate our use of the SMA (2). Our wish at this juncture is to determine that this approximation does not only possess a simple structure and provide numerical efficiency but also that it will give accurate representations of the problem that is being modelled. To do this we use the multi-mode approximation (MMA) that has previously been referred to, in which the SMA is extended through the addition of vertical modes that support purely evanescent waves, and in doing so arbitrarily close approximations of the full-linear solution can be obtained. This technique was employed by Bennetts [1] for two-dimensional problems with periodic geometry and we make use of the methods outlined therein. We may therefore use the full-linear solution generated by the MMA to assess the accuracy of our SMA.

Fig. 2 plots the modulus of the reflection coefficient against the frequency parameter K for two related problems, using both the SMA and the MMA. The geometrical variations are sinusoidal protrusions of amplitude 0.5 m that appear on the lower surface of an otherwise constant sheet of thickness 1 m. These variations are used in subsequent problems in this section and will be described more rigorously in due course. Part (a) shows results for geometry in which only one such period appears, whereas, in part (b), five such contiguous periods are used. The bed is flat throughout the infinite interval and lies at a depth of 20 m.

In Fig. 2 the SMA results are displayed by solid lines and those given using the MMA by crosses, where two additional vertical modes have been employed. The similarity between the results given by the SMA and those given by the MMA is striking. Only minute differences between the SMA and MMA may be detected, and, as may be anticipated, occur for small values of K. The findings presented here are typical of a wide range of results, and justify our use of the SMA in this work.

We now return to the issue of resonance, and will proceed using the SMA. Fig. 3 plots the build-up of resonance in the non-dimensionalised reflection coefficient $|R/I|$ about the first three Bragg values, $K = 1, 2, 3$, as the number of periods that make up the interval of varying geometry increases up to $M = 10$. The three subfigures give results for differing geometries. In each, the geometrical variations for an individual period are constant except for one surface, with: (a) $d(x) = Aq(x)$; (b) $D(x) = D_0 + Aq(x)$, $d = 0$; (c) $h(x) = h_0 + Aq(x)$, where

$$q(x) = \sin^2\left(\frac{\pi x}{l_1}\right), \tag{38}$$

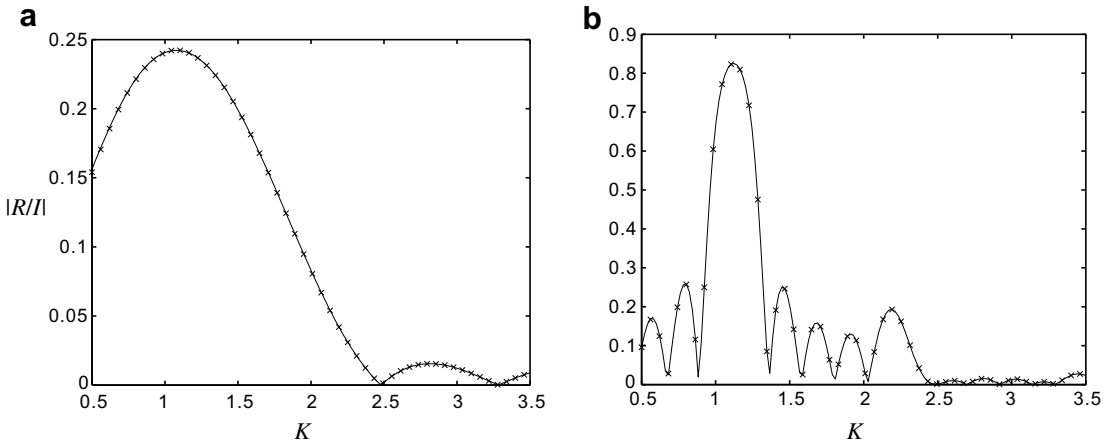

Fig. 2. The modulus of the reflected amplitude as a function of a frequency parameter. The geometrical variations appear on the lower surface of the plate and are of the form (38), where the thickness $D_0 = 1$ m and the amplitude is such that $A/D_0 = 0.5$. In part (a) one period is used ($M = 1$) and in part (b) five are used ($M = 5$). Results calculated from the SMA are shown by the lines and from the MMA (using one propagating mode and two evanescent modes) are shown by the crosses. The fluid depth is $H_0 = 20$ m.

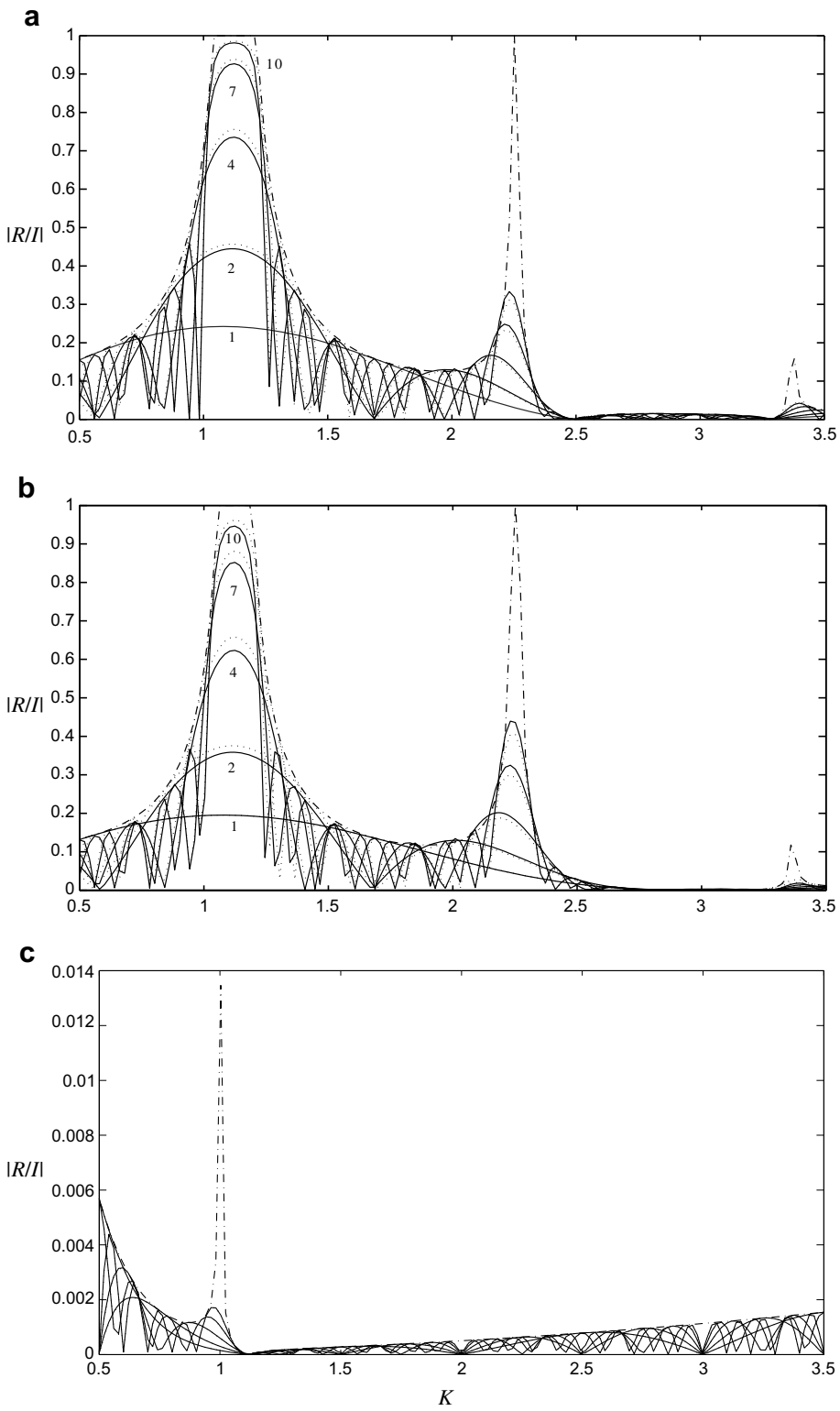

Fig. 3. The modulus of the reflected amplitude as a function of a frequency parameter. Each period is of the form (38) and results are shown for an interval of 1, 2, 4, 7 and 10 periods (solid curves). We use an ice thickness of $D_0 = 1$ m and fluid depth $H_0 = 10$ m. The variation appears as (a) a protrusion on the lower surface of the sheet ($A/D_0 = 0.5$); (b) a protrusion on the upper surface of the sheet ($A/D_0 = 0.5$); and (c) a protrusion on the bed ($A/H_0 = 0.25$). Corresponding results are shown for the plane wave approximation (dotted curves) and envelope (dot–dash).

which cause the variations to appear on the lower surface of the sheet, the upper surface of the sheet and the bed, respectively.

For the purposes of our results K will vary through the wavenumber k_0. The length of a period is fixed as $l_1 = 2\pi$. We also set the thickness $D_0 = 1$ m and fluid depth $H_0 = 10$ m in this figure.

Results are given for both the SMA formulated in Sections 3.2–3.3 (solid lines), and the PWA of Section 3.4 (dotted), along with the bounding envelope of Eq. (37) (dot–dash).

It is clear in parts (a) and (b), in which the variations take the form of protrusions in the sheet with amplitude $A = 0.5$ m, that the modulus of the reflection coefficient tends to 1 around the Bragg values as the number of periods increases. As in previous studies of periodic structures the resonances are strongest for the primary Bragg values and diminish at higher orders. We note that the resonant effects here are more pronounced than those seen for free-surface problems. Even for these modest protrusions we find that only a small number of periods is needed for the results to display a large response around primary and secondary Bragg resonances, and that large capture bands develop around these points. Furthermore, resonant effects are visible up to the third Bragg value.

The approximations given by the PWA display excellent accuracy in these figures, and it would be reasonable to study the results in terms of this simplified approximation if need be. However, their validity would diminish as the size of the obstruction increases. It follows that the bounding envelope provides a useful estimate of the maximum reflection caused of the periodic structure, enabling us to determine the positions and band-widths of resonances.

It may be observed that the results for the two geometries (a) and (b) are nearly identical. This feature has been noted previously by Bennetts et al. [2], and for this reason we will not consider variations in the upper surface of the sheet for the remainder of our results.

Another feature that is of interest is the drift in the resonance bands away from the Bragg values. This phenomenon is well known in analogous free-surface problems with periodic bedforms (see for example [11]). Drift in these situations has been commonly reported in a leftward direction. However, it is now clear that this effect results from the particular models of ripple beds that were used to compare theoretical predictions with the experimental data of [5]. In the results shown here, a clear tendency for a rightward movement is evident, and in light of these results the ripple bed case is being revisited as a separate theoretical investigation. We will conduct further study into the generation of drift at a later stage in this section.

In part (c) we see the results for a periodic protrusion in the bed, where we have increased the amplitude to $A = 2.5$ m. We can clearly see from this figure how little reflection is caused by the bed variation in comparison to the variations in the sheet. In particular note the scale on the vertical axis here. The PWA is omitted from this figure to avoid clutter.

It appears that the presence of the plate almost entirely dominates the rôle of the bed variations. Unsurprisingly then, very little evidence of Bragg resonance is seen for periodic topography in the presence of the plate. The only sign of resonance is a sharp peak in the bounding envelope at the primary Bragg value, which indicates that some resonance would occur if an increased number of periods were used, although it would still be negligible in comparison to that caused by the plate variations.

In Figs. 4 and 5 we explore the resonances seen in Fig. 3a in more detail. Fig. 4 shows the modulus of the plate displacement function, $|\eta|$, over the interval of varying geometry at three different values of the frequency parameter K, as it passes through the primary resonance. Situations in which no resonance occurs are shown in parts (a) and (c). We see, for these frequencies, that the displacement remains bounded as the number of periods increases. In comparison, for the frequency that lies within the resonance band, which is shown in part (b), the amplitudes of the flexural-gravity waves travelling through the plate grow as the number of periods gets larger. Moreover, we note that the amplitude of the wave travelling through the plate decays the further it gets from the entry point. This is true even in the case of a single period $M = 1$. We interpret this as an inability of the incident wave to penetrate through the obstruction, hence causing the large reflection that we saw in Fig. 3a at this and surrounding frequencies.

In Fig. 5 we study the eigenvalues of the associated transfer matrices for the problem considered in Fig. 3a, over the interval $K \in (0.5, 2.5)$. Part (a) plots the eigenvalues of the transfer matrix used in the PWA, for which we have the explicit expressions $e^{\pm i\lambda}$, where λ is calculated from Eq. (35). As predicted earlier, initially we see that as the frequency varies the two eigenvalues traverse the perimeter of the unit circle as a conjugate pair. However, as the eigenvalues approach the real axis at the point -1 from their respective directions, they depart from the unit circle for a finite interval and form a real-reciprocal pair, before returning to the unit circle and continuing their paths. The interval over which the eigenvalues do not occupy the unit circle defines the interval of primary resonance as indicated by the PWA. This process is repeated as the eigenvalues approach the value 1, although the departure is over a shorter interval. This corresponds to the secondary resonance being weaker than the primary one.

Part (b) plots the modulus of the eigenvalues of the transfer matrix P_1 used in the SMA and for which we do not have explicit expressions. There are six eigenvalues of P_1 but, as discussed in Section 3.3, we may restrict our attention to the three that make up the diagonal matrix Δ. The values of the remaining three are simply given by taking their inverses, which are the diagonal elements the matrix Δ^{-1}. Furthermore, we find that two of the eigenvalues that make up Δ are a conjugate pair and therefore have the same modulus. Hence, this figure comprises only two moduli. The graph shows that the modulus of the conjugate pair of eigenvalues is always less that unity and decreases with increasing frequency and that the modulus of the other eigenvalues mirrors that of the PWA eigenvalue whose modulus is less than unity. That is, its modulus is unity at all points away from resonance. In these intervals it departs from the unit circle and lies

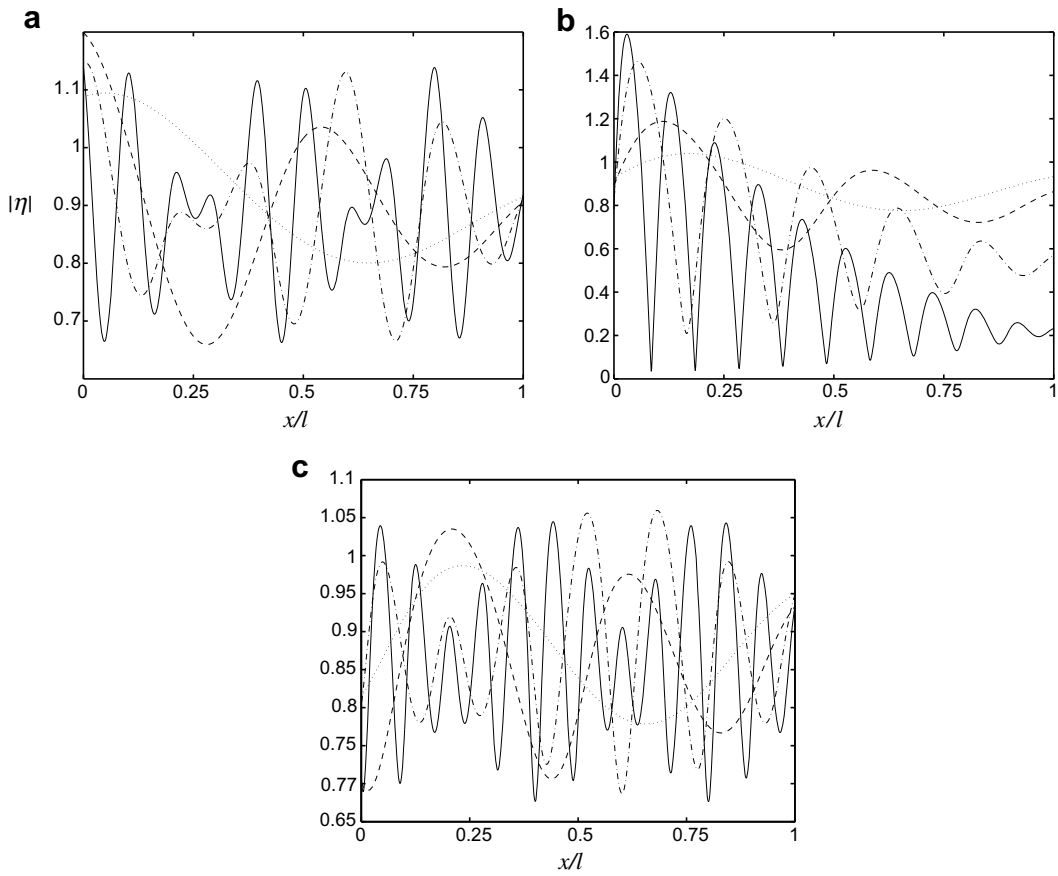

Fig. 4. The modulus of the displacement function over the interval of varying geometry for three different values of the frequency parameter as it passes through a primary Bragg resonance. In figure (a) $K = 0.81$, (b) $K = 1.17$ and (c) $K = 1.42$. The geometry is as in Fig. 3(a) and the number of periods are $M = 1$ (dotted curves), $M = 2$ (dashed), $M = 5$ (dot–dash) and $M = 10$ (solid).

on the real axis with a modulus less than one. The corresponding eigenvalue in Δ^{-1} (not shown) therefore also departs the unit circle at these points and lies on the real axis but with modulus greater than 1. It is clear then that this process is fundamental to the issue of resonance.

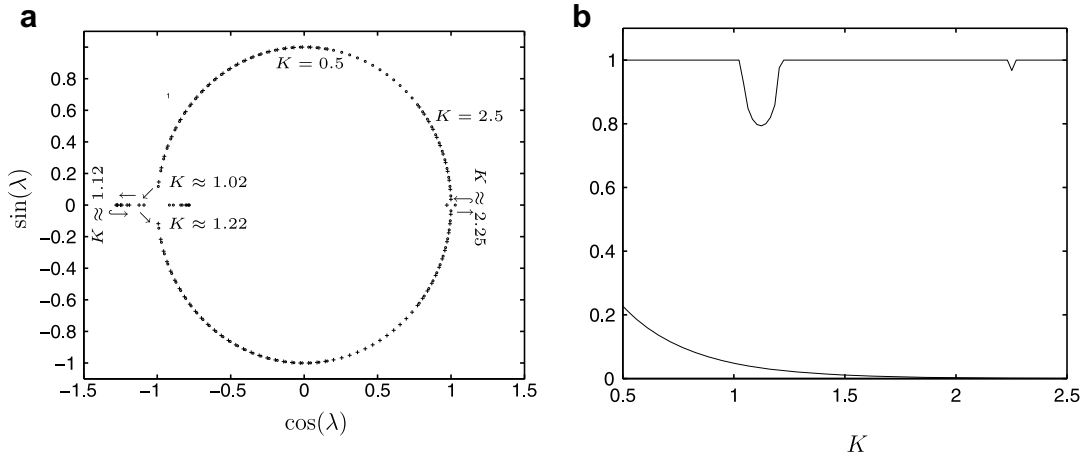

Fig. 5. The eigenvalues of the transfer matrices corresponding to Fig. 3(a) in the interval $K \in (0.5, 2.5)$. Part (a) is the eigenvalues $e^{\pm i\lambda}$ of the transfer matrix P_1, used in the PWA. Here the values of K shown and arrows refer to the eigenvalue denoted by the $+$ signs. Part (b) is the modulus of the two of the eigenvalues of $\mathscr{P}_1$, used in the full approximation, which appear in the matrix Δ.

For the remainder of the results that will be given here we return attention to the reflected amplitude, R, and look specifically at the influence on this value of the shape and relative magnitude of the geometrical obstacle. As we are no longer concerned with the build-up of resonance, and from here on, in each case, the interval of varying geometry is composed of five identical periods.

In Fig. 6 we again consider protrusions on the underside of the plate of the form (38) and how the relative size of these protrusions affect the scattering they cause. Part (a) shows three examples of the modulus of the reflected amplitude where the protrusions are of 0.5m amplitude, and ambient ice thicknesses of $D_0 = 0.1$ m (solid line), 0.5 m (dotted) and 1 m (dot–dash) are used. In comparison, in part (b) the thickness $D_0 = 1$ m is maintained for the three amplitudes 0.1 m (solid line), 0.5 m (dotted) and 1 m (dot–dash).

For all of the cases shown the five periods create significant resonance around the Bragg values. We can see that as the size of the protrusion increases in relation to the ambient thickness, the strength of the reflection becomes greater, particularly around the resonances. This is most evident for the 1m amplitude and $D_0 = 1$ m case shown in part (a), where we note that there is full resonance ($|R/I| \approx 1$) over a large band for the primary resonance. As the relative size of the obstruction increases we note also that the rightward drift, which we commented on earlier, becomes more prominent. An increase in drift resulting from a larger obstruction is consistent with observations in free-surface problems.

In Fig. 7 we conduct a similar investigation but with the protrusion appearing on the bed, beneath an uniform sheet. Part (a) plots the reflection coefficient for an amplitude of 2.5 m on a bed of depth 10 m, for the three thicknesses $D_0 = 0.1$ m, 0.5 m and 1 m. Here we see that as the plate becomes thinner it restricts the reflection caused by the topography less for the smaller values of the frequency parameter but for larger values the results are identical. However, the increase in reflection is only minimal and, as in Fig. 3, we note the vertical scale. In part (b) the amplitude 2.5 m is retained and we take the bed depths $H_0 = 10$ m, 7 m and 4 m beneath a plate of thickness $D_0 = 0.5$ m. The effect of raising the bed is strong and we see a significant amount of reflection for the most shallow case $H_0 = 4$ m, with clear evidence of both primary and secondary resonance.

As we have already discussed, the feature of rightward drift is something that has been largely neglected in water-wave models. However, recently (in work that is currently in preparation) Biggs has discovered this phenomenon in the case of free-surface flows. In Fig. 8 we investigate this issue further by studying alternative geometries. Again the plots are of the modulus of the reflection coefficient where the varying interval is composed of five periods. In part (a) each period is of the form given in Eq. (38) and, as in Fig. 6, these appear on the underside of the plate. However in this case they are indentations rather than protrusions, that is $d(x) = -Aq(x)$, and we use the amplitudes $A = 0.1$ m and 0.5 m. The effect of inverting the variation is to change the direction of the drift from rightward to leftward, which indicates that it is the property of the plate being thinner or thicker within each period that governs the direction of the drift. This is consistent with the findings of Biggs, who has shown that when the sheet is absent, rightward drift is caused by periodic troughs on the fluid bed, whereas leftward drift is caused by periodic protrusions on the fluid bed.

Motivated by the results of part (a), in part (b) we choose the sinusoidal variation $d(x) = -As(x)$

$$s(x) = \sin\left(\frac{2\pi x}{l_1}\right) \tag{39}$$

to be on the bottom of the plate, and again use amplitudes 0.1 m and 0.5 m. In the variation defined by Eq. (39) the indented and protruding parts are even, so that the influence of the thinning and thickening of the plate is neutral. We note here that

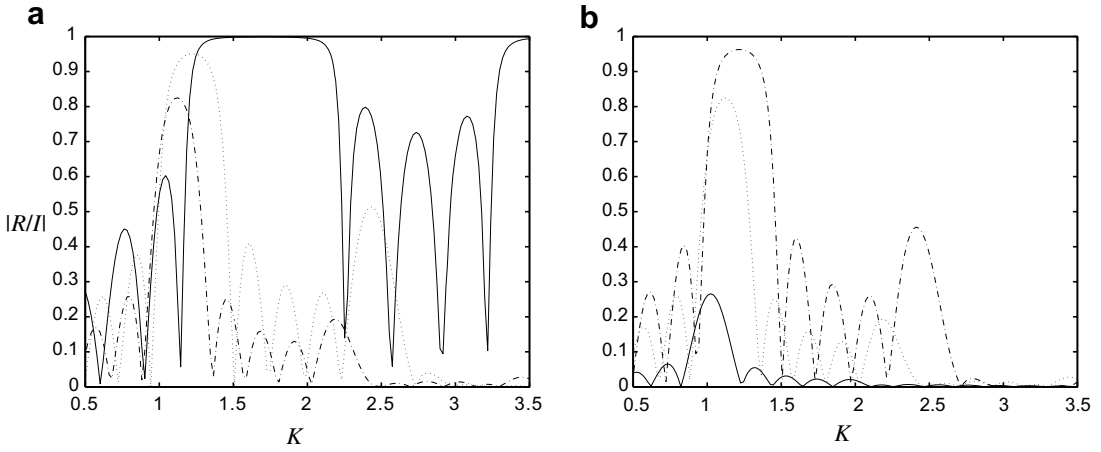

Fig. 6. The modulus of the reflected amplitude as a function of the frequency parameter. The interval of varying geometry is built-up from five identical periods where each period is as in Eq. (38) and appears as a protrusion on the underside of the plate. In part (a) $H = 10$ m, $A = 0.5$ m and three thicknesses $D = 0.1$ m, $D = 0.5$ m and $D = 1$ m are used. In part (b) $D = 1$ m, $H = 10$ m and three amplitudes $A = 0.1$ m, $A = 0.5$ m and $A = 1$ m are used.

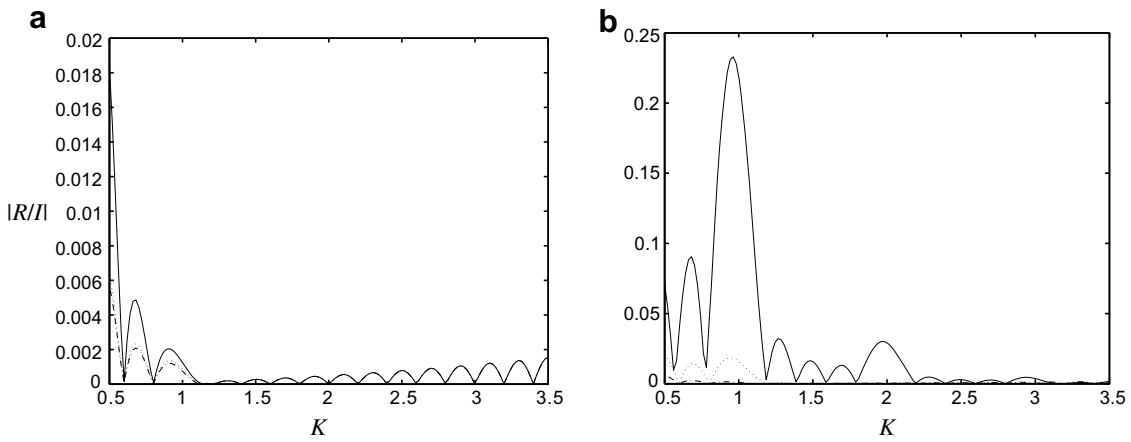

Fig. 7. As in Fig. 6 but with the variation appearing as a protrusion on the bed. In part (a) $H = 10$ m, $A = 2.5$ m and three ice thicknesses $D = 0.1$ m, $D = 0.5$ m and $D = 1$ m are used. In part (b) $D = 0.5$ m, $A = 2.5$ m and fluid depths $H_0 = 4$ m, $H_0 = 7$ m and $H_0 = 10$ m are used.

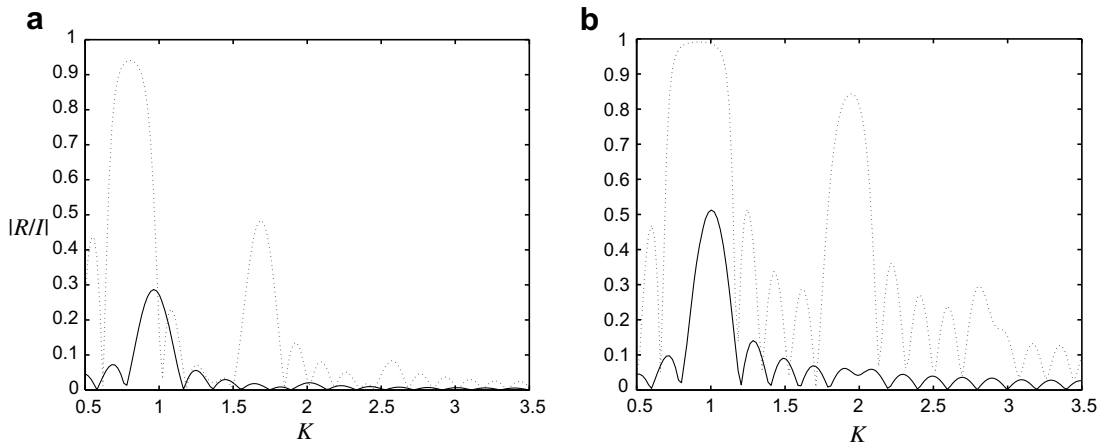

Fig. 8. Part (a) is as in Fig. 6 but where the variation appears as an indentation in the underside of the plate. Part (b) is as in Fig. 6 but where each period is defined by Eq. (39).

despite the fact that the overall reflection increases compared to part (a), the drift is far less pronounced. However, visible drift is still evident in the leftward direction. We therefore conclude that the tendency in the absence of a preference for thinning or thickening of the plate is for leftward drift.

5. Conclusions

In this work we have considered a specific class of two-dimensional problems involving an elastic plate floating on a fluid domain. Our investigation has been into the case in which an incident flexural-gravity wave is scattered by a finite interval of varying geometry that is built-up of a finite number of identical periods.

To do this we invoked a mild-slope approximation, in which the vertical dependence of the velocity potential is based on the mode that supports incident waves for uniform geometry. The existence of an elastic plate induces oscillatory-evanescent waves that are not present in the free-surface case.

The SMA is obtained by solving a sixth-order ODE. A solution procedure for such a problem has been outlined in previous investigations of fluid-plate systems. These methods rely on the discretisation of the entire interval of varying geometry. However, our interest in this work differed from that of these authors, as we wished to study the build-up of resonance as the number of identical periods was increased. We therefore set-out to construct a new solution method, from which we could gain the solution for an arbitrary number of periods from the numerical calculation of the ODEs over a single such period. This constituted a significant computational efficiency.

A method was created through the use of transfer matrices. Transfer matrices relate the amplitudes of the outgoing and incoming waves on either side of a geometrical period, unlike the more common scattering matrices that relate outgoing waves to incoming waves. This allowed us to easily compose the scattering between adjacent periods and adjoin an arbitrary number of periods. Such use of transfer matrices has been applied previously to free-surface flows; however, in this case we must consider the interaction of oscillatory-evanescent waves with the propagating waves.

In addition to its efficiency, the method of transfer matrices also allows for greater analytical insight into the process of resonance. To this end, we conducted an investigation of the transfer matrix and derived certain properties, which also proved to be of practical use for structures consisting of a large number of periods. It was shown that the eigenvalues of the transfer matrix come in reciprocal and conjugate pairs. However, the presence of the oscillatory-evanescent waves meant that explicit links between the eigenvalues and resonance could not be drawn.

Motivated by a wish to have a simple, explicit expression for the scattering coefficients and to study the effect of the oscillatory-evanescent waves on the passage of the propagating waves, we created a simplified approximation. In this simplified approximation the only interaction that is considered between adjacent periods is that of the propagating waves, and we described this as the plane-wave approximation (PWA). The PWA is identical in structure to approximations used on free-surface flows and we were therefore able to use this existing work to aid our analysis. An explicit link was drawn between the eigenvalues of the transfer matrix departing the unit circle and the production of resonance as the number of periods used increases, and bounding envelopes for the approximate scattering coefficients were given.

We gave a set of numerical results in which we studied the build-up of resonance with increasing periods around the so-called Bragg values. It was seen that pronounced Bragg resonance was produced by a relatively small number of periods and modest variations when the obstruction occurred on the plate. Particularly striking was the large capture bands of resonance here. In contrast, the presence of the plate served to subdue the reflection caused by bed undulations, so that resonance was only seen in extreme cases.

A new feature of displacement of the resonance bands in the rightward direction was seen in the numerical results. Drift of the peak of resonance away from the Bragg values occurs as the relative size of the obstruction increases. It is a well-established phenomenon in free-surface flows over period bedforms in a leftward direction, although it has recently been established that rightward drift also exists in free-surface problems. We were able to draw a link between plates that become thinner in the varying interval and leftward drift and plates that become thicker in the varying interval and rightward drift. It was further shown that in the absence of overall thinning/thickening the tendency is for leftward drift.

It may be possible to pursue the issue of drift analytically. This would most likely be done through a perturbation method. However, the high order of the ODE system, coupled with the large number of parameters that appear in the problem would be likely to complicate matters.

Related periodic geometries could also be investigated using transfer matrices. For instance, we may consider the case of a finite number of floating plates on an otherwise unloaded fluid surface. Furthermore, transfer matrices may be applied to the problem of an array of fully three-dimensional plates, where the array is infinite in one direction and finite in another, and this is currently in preparation. This work is related to that of [10], who solved for gravity waves over a structure of varying topography in a periodic rectangular lattice.

References

[1] L.G. Bennetts, Wave scattering by ice sheets of variable thickness. PhD thesis, University of Reading, UK, 2007.
[2] L.G. Bennetts, N.R.T. Biggs, D. Porter, A multi-mode approximation to wave scattering by ice sheets of varying thickness, J. Fluid Mech. 579 (2007) 413–443.
[3] P.G. Chamberlain, D. Porter, Decomposition methods for wave scattering by topography with application to ripple beds, Wave Motion 22 (1995) 201–214.
[4] I.F. Collins, I.R. McCrae, Creep buckling of ice shelves and the formation of pressure rollers, J. Glaciol. 31 (1985) 242–252.
[5] A.G. Davies, A.D. Heathershaw, Surface-wave propagation over sinusoidally varying topography, J. Fluid Mech. 245 (1984) 301–317.
[6] D. Evans, R. Porter, Scattering of flexural waves by multiple narrow cracks in ice sheets floating on water, Wave Motion 43 (5) (2006) 425–443.
[7] C. Fox, A scaling law for the flexural motion of floating ice, in: J.P. Dempsey, H.H. Shen (Eds.), Proceedings of IUTAM Symposium on Scaling Lams in Ice Mechanics and Ice Dynamics, Kluwer Academic, Dordrecht, 2001, pp. 135–148.
[8] C.C. Mei, T. Hara, M. Naciri, Note on Bragg scattering of water waves by parallel bars on the seabed, J. Fluid Mech. 186 (1988) 147–162.
[9] M.A. Peter, M.H. Meylan, C.M. Linton, Water-wave scattering by a periodic array of arbitrary bodies, J. Fluid Mech. 348 (2006) 237–256.
[10] D. Porter, R. Porter, Interaction of water waves with three-dimensional periodic topography, J. Fluid Mech. 434 (2000) 301–335.
[11] D. Porter, R. Porter, Scattered and free waves over periodic beds, J. Fluid Mech. 483 (2003) 129–163.
[12] D. Porter, R. Porter, Approximations to wave scattering by an ice sheet of variable thickness over undulating topography, J. Fluid Mech. 509 (2004) 145–179.
[13] V.A. Squire, Of ocean waves and sea-ice revisited, Cold Reg. Sci. Technol. 49 (2) (2007) 110–133.
[14] V.A. Squire, J.P. Dugan, P. Wadhams, P.J. Rottier, A.K. Liu, Of ocean waves and ice sheets, Ann. Rev. Fluid Mech. 27 (1995) 115–168.
[15] C. Wang, M.H. Meylan, R. Porter, The linear wave response of a periodic array of floating elastic plates, J. Eng. Math. 57 (1) (2007) 23–46.
[16] E. Watanabe, T. Utsunomiya, C.M. Wang, Hydroelastic analysis of pontoon-type VLFS: a literature survey, Eng. Struct. 26 (2) (2004) 245–256.
[17] T.D. Williams, V.A. Squire, Oblique scattering of plane waves by heterogeneities in sea-ice, Proc. Roy. Soc. (A) 460 (2004) 3469–3497.